crystals

MDPI

Article

Origins of a Low-Sulfur Superalloy Al_2O_3 Scale Adhesion Map

James Smialek †

NASA Glenn Research Center, Cleveland, OH 44135, USA; dr.jsmialek@outlook.com
† Retired.

Abstract: Low-sulfur single-crystal Ni-base superalloys have demonstrated excellent cyclic oxidation resistance due to improved Al_2O_3 scale adhesion. This derives from preventing deleterious interfacial sulfur segregation that occurs at common ppm levels of S impurity. Multiple hydrogen-annealing desulfurization treatments were employed to produce a continuum of levels demonstrating this oxidative transition, using 1 h cyclic oxidation at 1100 °C for 500 h to 1000 h. The sulfur content was determined by glow discharge mass spectrometry. The complete gravimetric database of 25 samples is revealed and correlated with sulfur content. Maximum adhesion (i.e., no weight loss) was achieved at $\leq$ 0.3 ppmw S, significant spallation (20–30 mg/cm^2) above 2 ppmw, with transitional behavior between 0.3 and 2 ppmw S. A map suggested that adhesion was enabled when the total sulfur reservoir was less than one S atom per Ni interface atom. Equilibrium models further suggest that segregation may be minimized (~1% at 0.2 ppmw bulk), regardless of section thickness. 1st order adhesion effects have thus been demonstrated for PWA 1480 having no Y, Zr, or Hf reactive element dopants and no possibility of confounding reactive element effects. The results are compared with 2nd generation PWA 1484, Rene'N5, N6, and CMSX-4® SLS, all having Hf dopants.

Keywords: scale adhesion; sulfur segregation; superalloys; cyclic oxidation

Citation: Smialek, J. Origins of a Low-Sulfur Superalloy Al_2O_3 Scale Adhesion Map. *Crystals* **2021**, *11*, 60. https://doi.org/10.3390/cryst11010060

Received: 18 December 2020
Accepted: 11 January 2021
Published: 13 January 2021

1. Introduction

Al_2O_3-forming coatings and superalloys are widely accepted as among the most oxidation-resistant high-temperature materials used commercially. In addition to low scale growth rates, the materials must also possess good scale adhesion to prevent spallation and wastage caused by thermal cycling. Generally, this was spectacularly accomplished through reactive element dopants, Y, Zr, Hf, etc. Among numerous other theories, it was postulated that these elements served to getter ppm levels of a sulfur impurity, thus preventing deleterious interfacial segregation and bond weakening. Upon cooldown, significant compressive thermal stress produces spallation of the scale, with concurrent loss of alloy Al content. This may proceed initially with some gradual weight loss in repeated thermal cycling exposures. However, more seriously, continued cycling allows a transition to other oxides that grow much faster and eventually produce breakaway oxidative degradation.

In order to support this mechanism, various methods were explored to produce low sulfur materials with improved cyclic oxidation behavior. The significant effect of low sulfur content on the cyclic oxidation and spalling behavior of high-temperature alloys has been well established. Initially, studies were on cyclic polish-purged NiCrAl alloys, where improved adhesion was initiated at low sulfur contents on the order of 1 ppmw. These transitioned to single-crystal alloys and the use of 1 atm hydrogen annealing as a more efficient, controlled desulfurization technique [1,2]. As this process was refined, multiple PWA 1480 (Pratt and Whitney, East Hartford, CT, USA) single-crystal samples were desulfurized by adjusting the thickness of the sample and time/temperature of the anneal. Correlation of the desulfurization conditions with cyclic oxidation [3] provided the source data for this paper. At that time, the only sulfur content available was that predicted by the thin slab diffusion solution. The corresponding measured sulfur contents

were reported elsewhere [4]. While these values were embedded in subsequent reviews [5], a full disclosure of the oxidation results and sulfur contents of each sample was never explicitly provided.

It is the purpose of the present paper to revisit and fully present the results of this 25-sample matrix to allow a detailed examination of all the gravimetric results, now coupled with specific sulfur contents. Broader adhesion aspects related to various proposed reactive element effects are beyond the scope of this paper. PWA 1480 does not contain any Y, Hf, or Zr dopants, which cannot play a role here. Related discussions have been presented with appropriate referencing [5].

Lastly, the results are compared to updated cyclic oxidation results for low sulfur hydrogen-annealed 2nd generation single-crystal superalloys PWA 1484, Rene' N5, N6, and melt-desulfurized CMSX-4® SLS (super low sulfur) (Pratt and Whitney, East Hartford, CT, USA; General Electric Corp., Evendale, OH, USA; Cannon-Muskegon Corp., Muskegon, MI, USA). The latter all exhibited superior cyclic oxidation behavior at 1100 °C and above. In short, this note highlights the numerical cyclic oxidation data of single-crystal superalloys as improved when extremely low levels of sulfur (0.2 ppmw) are approached.

2. Materials and Methods

A polycrystalline ingot of PWA 1480 melt stock was sectioned by electro-discharge machining (EDM) into rectangular samples of various thicknesses. The overall dimensions were ~12.7 ×25.4 mm ($\frac{1}{2}$ x 1″). The machined thicknesses were nominally 0.25, 0.51, 1.27, 2.54, and 5.08 mm (labeled "10, 20, 50, 100, and 200 mils"). They were further hand polished on SiC emery paper down to 600 grit. Hydrogen annealing took place in a horizontal alumina tube under slowly flowing 5% H_2/Ar, using Zr foil as an oxygen getter. Four temperatures, 1000 °C, 1100 °C, 1200 °C, and 1300 °C, were used. Times were 8, 20, 50, or 100 h. Annealing weight changes were less than 0.03 mg/cm^2 as samples were clean and metallic in appearance (no surface scale). Samples had a 1.5 mm slice taken from the end for sulfur analyses by glow discharge mass spectroscopy (GDMS, Shiva Technologies, Syracuse; now Evans Analytical Group, EAG, Liverpool, NY, USA). Samples were repolished as before, re-measured, and tested by cyclic oxidation in a vertical alumina tube furnace at 1100 °C (1 h heating and 10 min cooling). Weight change was monitored on a Sartorius analytical balance, sensitive to 0.01 mg. Balance drift was periodically checked using standard 1.00000 and 5.00000 g weights. Scales were examined by XRD and SEM with results highlighted previously [1–5].

3. Results and Discussion

3.1. Cyclic Oxidation vs. Sulfur Database

The cyclic oxidation results were tabulated for the series of sample thicknesses, as delineated by annealing temperature/time. These are presented in Tables 1–4 for nominally "10 mil", "20 mil", "50 mil", "100 mil" and "200 mil" samples (0.15, 0.42, 1.22, 2.53, and 5.02 mm actual thickness). The sulfur content of the starting material was ~6.15 ppmw; that of the annealed samples is also included. These complete data sets allow for multiple analysis schemes, as opposed to simply presenting representative plots. It can be seen in Table 1 that significant weight losses occurred after 500 h oxidation for the "10 mil" samples (polished to ~0.15 mm) hydrogen-annealed at 1000 °C for 20 h or less. Oxidation resistance improved for 100 h anneals and achieved small gains for samples annealed at 1200 °C, indicating adherent behavior. Table 2 presents results for the "20 mil" samples (polished to ~0.42 mm), indicating a substantial −33 mg/cm^2 loss for the control (no anneal). It improved slightly with 1000 °C, and 1100 °C hydrogen anneals. They exhibited small gains for samples annealed at 1200 °C and only a modest loss for the sample annealed at 1300 °C (samples annealed at 1300 °C may exhibit anomalous behavior because they suffered incipient melting during the anneal and may not represent master ingot microstructure). Duplicate samples annealed for 20 h both showed small 0.6 mg/cm^2 gains after 500 h, with one decreasing to near 0 mg/cm^2 after 1000 h. The "50 mil" samples (~1.22 mm), Table 3,

showed the highest 500 h weight losses (−66 mg/cm^2) for the control sample, i.e., with no hydrogen anneal. Annealing at 1200 °C produced progressively less oxidative weight loss with annealing time, achieving a small weight gain for the 100 h annealed sample. The "100 mil" samples (~2.53 mm), Table 4, exhibited weight loss for samples hydrogen-annealed at 1100 °C and 1200 °C, the latter with some improvement for 100 h annealing. The 1300 °C annealing appeared to produce an improved performance here. Finally, the "200 mil" samples (~5.09 mm) exhibited various degrees of non-adherent behavior for both the 1200 °C and 1300 °C-annealed samples.

Table 1. Cyclic-oxidation specific weight change data for "10 mil" PWA 1480 samples (1100 °C for 500 h in air). Effect of hydrogen annealing time and temperature. Measured sulfur content (C_S) after hydrogen annealing; thickness (L) measured after polishing and before oxidation testing.

Sample #	**10-7**	**10-6**	**10-1**	**10-2**	**10-4**
L, mm	0.18	0.18	0.12	0.14	0.18
H_2, (°C/h.)	1000/8	1000/20	1000/100	1200/20	1200/100
h.\C_S (ppmw)	4.9	4.6	4.3	0.15	0.07
0 h	0.00	0.00	0.00	0.00	0.00
1	0.25	0.23	0.20	0.21	0.23
5	0.03	0.26	0.23	0.26	0.27
10	0.07	0.00	0.25	0.29	0.29
20	−0.21	−0.16	0.27	0.33	0.33
40	−1.32	−1.24	0.27	0.39	0.38
60	−2.14	−1.92	0.25	0.42	0.42
80	−2.98	−2.58	0.15	0.42	0.42
100	−3.77	−3.21	0.03	0.46	0.46
150	−5.48	−4.86	−0.27	0.52	0.52
200	−6.95	−5.98	−0.70	0.56	0.57
250	−9.24	−7.41	−1.06	0.58	0.60
300	−10.43	−8.78	−1.49	0.61	0.63
400	−13.48	−10.49	−2.35	0.60	0.65
500	−24.33	−18.35	−2.57	0.58	0.65

3.2. Cyclic Oxidation Plots

The cyclic oxidation weight change vs. time was plotted for many conditions [4]. They show variations of a classic cyclic oxidation form: initial parabolic weight gain, a small maximum less than 1 mg/cm^2, a gradual decrease to cross zero weight change, and a final, perhaps linear, rate of loss. An example is presented in Figure 1 for a full range of sulfur contents. This family of curves is for samples of various nominal thicknesses ("10 mil", "20 mil", and "50 mil"), annealed at various *T*, *t*, plus the un-annealed 6.7 ppmw S control sample baseline. Other figures illustrated the basic trend toward greater adhesion for thinner samples, higher annealing temperatures and longer annealing times [4]. These are keyed to the diffusion factor containing thickness (*L*) and time (*t*) as Dt/L^2 and in the temperature control of D_s as $D_s = D_0 \exp(-Q/RT)$. Although difficult to resolve because of overlapping curves, it is noted that early growth rates, before measurable spallation occurred, fall within a small range. The average 5-h data from 23 samples in Tables 1–4 (less two outliers) was 0.272 mg/cm^2, with a standard deviation of 0.065 (i.e., 24%). These low values suggest no significant change in growth mechanism occurred in the initial Al_2O_3 films. This is contrasted with ~5000% differential in final weight change, e.g., −30 mg/cm^2 vs. +0.6 mg/cm^2.

Table 2. Cyclic-oxidation specific weight change data for "20 mil" PWA 1480 samples (1100 °C for 500 or 1000 h in air). Effect of hydrogen annealing time and temperature. Measured sulfur content (C_S) after hydrogen annealing; thickness (L) measured after polishing and before oxidation testing.

Sample #	**20-0**	**20-1**	**20-8**	**20-5**	**20-3**	**20-4**	**20-9**	**20-6**	**20-7a**	**20-2**
L. mm	0.42	0.45	0.44	0.43	0.41	0.39	0.39	0.42	0.42	0.40
H_2, (°C/h.)	none	1000/20	1100/20	1200/8	1200/20	1200/20	1200/50	1200/100	1200/100	1300/20
h.\C_S (ppmw)	6.7	3.9	2.1	0.8	0.28	N.A.	0.05	0.08	0.2	0.06
0 h	0.00	0.00	0.00	0.00	0.00	0.00	0.00	0.00	0.00	0.00
1	0.23	0.23	0.24	0.23	0.23	0.22	0.21	0.21	0.16	0.23
5	0.28	0.30	0.27	0.27	0.26	0.25	0.25	0.25	0.21	0.25
10	0.27	0.26	0.32	0.29	0.31	0.30	0.29	0.27	0.24	0.28
20	−0.16	0.15	0.32	0.33	0.32	0.31	0.33	0.30	0.30	0.32
40	−1.18	−0.65	0.01	0.36	0.36	0.35	0.39	0.34	0.37	0.34
40	−1.25	−0.72	−0.07	0.32	0.37	0.35	0.39	0.34	0.35	0.33
60	−2.73	−1.85	−1.05	0.10	0.52	0.50	0.52	0.44	0.49	0.34
80	−3.24	−2.27	−1.92	0.07	0.53	0.53	0.54	0.46	0.52	0.31
100	−3.98	−3.25	−2.97	−0.01	0.55	0.54	0.55	0.47	0.53	0.29
150	−5.64	−4.83	−4.70	−0.16	0.57	0.58	0.60	0.51	0.57	0.24
200	−7.44	−6.07	−6.27	−0.34	0.62	0.62	0.65	0.54	0.61	0.16
200	−8.01	−6.42	−6.61	−0.48	0.57	0.57	0.60	0.49	0.60	0.03
250	−12.08	−9.13	−9.46	−0.81	0.58	0.59	0.60	0.50	0.59	−0.05
300	−15.32	−12.61	−12.85	−1.11	0.62	0.62	0.63	0.52	0.61	−0.14
400	−23.89	−18.18	−18.57	−1.79	0.63	0.65	0.63	0.49	0.65	−0.42
500	−32.55	−24.81	−25.85	−2.61	0.59	0.64	0.65	0.49	0.68	−0.77
500	−32.86	−24.99	−26.05	−2.67	0.58	0.62	0.67	0.46	0.65	−0.83
600				−3.28	0.52		0.57	0.39		−1.13
700				−3.77	0.49		0.54	0.37		−1.41
800				−4.37	0.45		0.50	0.35		−1.68
900				−5.22	0.31		0.46	0.31		−2.24
1000				−6.74	0.10		0.36	0.16		−3.38

Table 3. Cyclic-oxidation specific weight change data for "50 mil" PWA 1480 samples (1100 °C for 500 h in air). Effect of hydrogen annealing time and temperature. Measured sulfur content (C_S) after hydrogen annealing; thickness (L) measured after polishing and before oxidation testing.

Sample #	**50-0**	**50-4**	**50-3**	**50-5**	**50-2**
L, mm	1.20	1.19	1.18	1.24	1.27
H_2, (°C/h.)	control	1200/8	1200/20	1200/100	1300/20
h.\C_S (ppmw)	N.A.	2.0	1.5	0.12	0.34
0 h	0.00	0.00	0.00	0.00	0.00
1	0.20	0.22	0.24	0.22	0.04
5	0.30	0.26	0.29	0.26	0.07
10	0.25	0.20	0.33	0.30	0.10
20	−0.05	0.10	0.33	0.38	0.10
40	−0.98	−0.25	0.23	0.46	0.02
60	−1.95	−0.97	0.04	0.55	−0.14
80	−2.82	−1.81	−0.25	0.59	−0.29
100	−3.70	−2.65	−0.65	0.65	−1.06
150	−5.93	−4.71	−2.05	0.79	−2.03
200	−8.08	−6.78	−3.66	0.73	−3.08
250	−10.80	−8.92	−5.08	0.77	−4.17
300	−16.95	−11.93	−6.48	0.76	−6.39
400	−33.94	−23.21	−9.35	0.72	−6.39
500	−66.85	−37.90	−12.51	0.75	−8.68

Table 4. Cyclic-oxidation specific weight change data for "100 mil" and "200 mil" PWA 1480 samples (1100 °C for 500 h in air). Effect of hydrogen annealing time and temperature. Measured sulfur content (C_S) after hydrogen annealing; thickness (L) measured after polishing, before oxidation testing.

Sample #	100-2	100-1	100-3	100-4	200-1	200-2
L, mm	2.54	2.53	2.51	2.59	5.06	5.12
H_2, (°C/h.)	1100/100	1200/20	1200/100	1300/100	1200/100	1300/20
h.\C_S (ppmw)	2.1	1.5	0.4	0.01	1.4	3.3
0 h	0.00	0.00	0.00	0.00	0.00	0.00
1	0.31	0.29	0.33	0.30	0.24	0.25
5	0.35	0.33	0.38	0.36	0.28	0.34
10	0.39	0.36	0.44	0.40	0.31	0.34
20	0.43	0.33	0.49	0.43	0.26	0.23
40	0.38	0.17	0.53	0.50	0.15	−0.19
60	0.17	−0.01	0.53	0.53	−0.03	−0.79
80	−0.11	−0.36	0.53	0.55	−0.25	−1.45
100	−0.60	−0.98	0.45	0.55	−0.53	−2.22
150	−2.62	−2.79	0.10	0.53	−1.44	−3.88
200	−4.66	−4.41	−0.49	0.47	−2.75	−5.56
300	−8.90	−7.86	−2.07	0.34	−5.60	−9.29
400	−15.35	−11.97	−3.75	0.21	−8.34	−14.57
500	−26.34	−20.55	−5.67	0.06	−12.82	−27.52

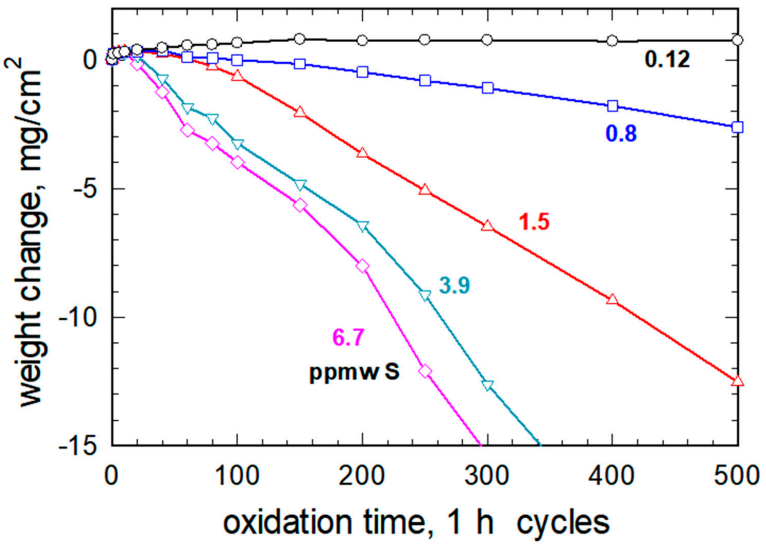

Figure 1. Selected family of 1100 °C, 1 h cyclic oxidation weight change curves for PWA 1480, showing increased attack with sulfur content and excellent scale-adhesion behavior at the 0.1 ppmw S level [6] (Curves correspond to samples 50-5, 20-5, 50-3, 20-1, and 20-0).

3.3. Correlation with Sulfur Content

For theoretical and practical purposes, it is instructive to catalog cyclic oxidation behavior as a function of sulfur content. The first attempt at a concise formulation may be to correlate a figure of merit with sulfur content. This had been done by plotting 500 h weight change vs. sulfur content [4]. While illustrating the overall trend, it was seen that plots for various sample thicknesses did not collapse on a single-valued, monotonic, universal curve. However, the data strongly suggested fully adherent behavior for sulfur contents at or below about 0.1 ppmw S for most thicknesses. It also suggested that thicker samples required lower sulfur contents to become adherent, and, conversely, thinner samples maintained adhesion at higher sulfur contents. Thus, a unique value of critical sulfur content could not immediately be claimed for all section thicknesses.

Since breakaway weight change may follow nonuniform, less repeatable behavior, a second attempt was made to correlate performance with sulfur content by using the time to cross zero weight change, i.e., t_0, as compiled in Table 5 for convenient reference. This construction is shown in Figure 2. Here each symbol *shape* refers to one section thickness, and fill color refers to one anneal temperature. It is seen that high sulfur contents are inevitably associated with short times to cross zero, t_0, as low as 20 h (lower right quadrant). At lower sulfur contents, below about 0.3 ppmw, most data points indicate nearly full adhesion (upper left quadrant), some not exhibiting any decrease in weight change over the entire test duration (i.e., t_0 > 500 h or 1000 h) (Red symbols, 1300 °C anneals, may indicate anomalous behavior as mentioned previously). The advantage of this construction is that a sharp edge ($\leq$ 0.3 ppmw S) is illustrated, separating excellent performance from the downward trend toward that exhibited by unannealed samples at ~6 ppmw S. While this representation provides a useful graphical tool, a more mechanistic approach might involve the rate of weight loss or a spall constant extracted from cyclic oxidation models, such as COSP [7].

Table 5. Correlation of cyclic oxidation behavior figures of merit with sulfur content (C_S) and sample thickness (L). PWA 1480, 500 h weight change ($\Delta W/A_{500}$) and time to cross zero weight (t_0). Sulfur content was initially reduced by annealing at 1000–1300 °C for 8–100 h in 5% H_2/Ar.

H_2: Temp.	**1000 °C**			**1100 °C**			**1200 °C**			**1300 °C**		
	C_s	**DW/A$_{500}$**	t_0	C_s	**DW/A$_{500}$**	t_0	**C$_s$**	**DW/A$_{500}$**	t_0	C_s	**DW/A$_{500}$**	t_0
H_2: Time	**ppmw**	**mg/cm^2**	**h**	**ppmw**	**mg/cm^2**	**h**	**ppmw**	**mg/cm^2**	**h**	**ppmw**	**mg/cm^2**	**h**
L = 0.15 mm												
8	4.9	−24.33	10									
20	4.6	−18.36	10				0.15	0.58	>500			
100	4.3	−2.57	100				0.07	0.65	>500			
L = 0.42 mm												
0	6.7	−32.86	20									
8							0.8	−2.62	100			
20	3.9	−24.99	20	2.1	−26.05	40	0.28	0.59	1050	0.06	−0.83	40
20							N.A.	0.64	>500			
50							0.05	0.65	1350			
100							0.08	0.68	1100			
100							0.2	0.49	>500			
L = 1.22 mm												
8							2	−37.90	20			
20							1.5	−12.52	60	0.34	−8.68	40
100							0.12	0.75	>500			
L = 2.53 mm												
20							1.5	−20.55	60			
100				2.1	−26.34	80	0.4	−5.67	150	0.01	0.06	500
L = 5.09 mm												
20										3.3	−27.52	40
100							1.4	−12.82	60			

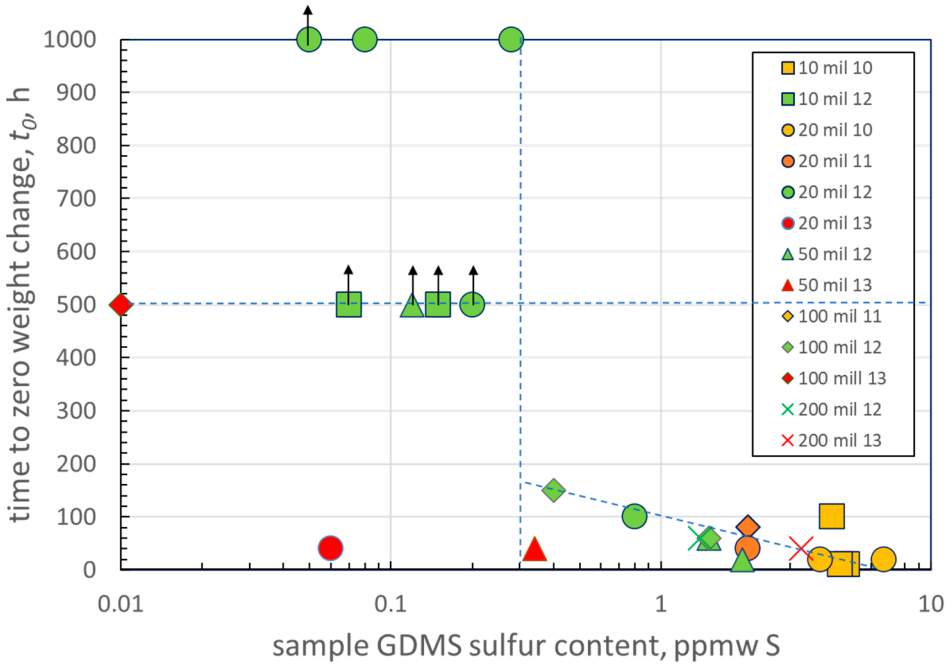

Figure 2. Cyclic oxidation performance scatter diagram for all PWA 1480 samples. The abrupt large increase in adhesion behavior (t_0, time to cross zero) for hydrogen-annealed samples having less than ~0.3 ppmw sulfur (1100 °C oxidation, up to 1000 h). Up arrows indicate t_0 condition not yet achieved. At higher sulfur levels, the overall trend indicates poor adhesion (lower t_0) with increasing sulfur content (symbols correspond to sample thickness, colors correspond to hydrogen anneal temperature: yellow 1000 °C, orange 1100 °C, green 1200 °C, red 1300 °C).

3.4. Scale-Adhesion Map

These results were influenced by sample thickness, first because desulfurization was limited for thick samples with a large diffusion distance. However, there is a secondary thickness consideration. It derives from the larger reservoir of residual sulfur contained in thick samples, even at equivalent sulfur content to thin samples. During cycling, this allows for more re-segregation after repeated spallation events that remove sulfur from the damaged interface. To accommodate this factor, an adhesion map was constructed that included sample thickness as a variable affecting the total sulfur content. The other variable was the GDMS measured sulfur content of each individual sample, with various hydrogen annealing pretreatments. The data were color-coded by regions of 500 h cyclic weight change behavior, from very adherent ($\pm$ 1 mg/cm^2) to poorest performance (<-30 mg/cm^2) and is shown in Figure 3. Furthermore, approximate positions of 0 and -10 mg/cm^2 were interpolated from data corresponding to each individual set of nominal thickness. This allowed a locus of initially adherent and non-adherent boundaries to be delineated, as indicated by the solid lines. These show a downward trend of lower sulfur content needed for thicker sections to produce adherent behavior. A simple example interpolates a critical sulfur content of ~0.2 ppmw for a 1 mm thick section.

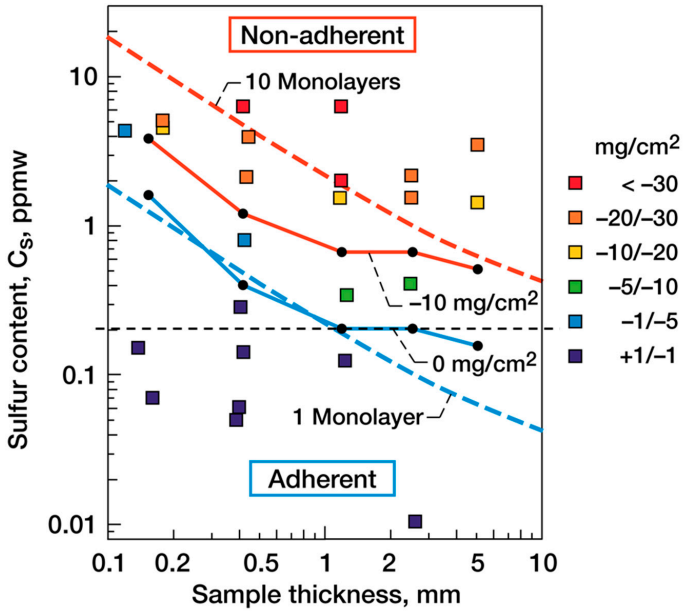

Figure 3. Cyclic oxidation adherence map for PWA 1480 [4] (1100 °C, 500 (1 h) cycles). Color coding indicates a trend to excellent performance (low weight change) for low sulfur samples and low thickness. Interpolated transition boundary (blue) correlates with a bulk sulfur reservoir equivalent to ~1 monolayer of total sulfur segregation. Projected McLean 1% surface coverage corresponds to 0.2 ppmw S bulk.

Lastly, a mass balance approach was applied to the total amount of sulfur contained in the sample as compared to the amount required to provide one full monolayer coverage due to interface segregation [4,6]:

$$C_S = (8.27 \times 10^{-2}\ \mathrm{gm/cm^2})\ N_m\ (A/W) \quad (1)$$

where C_S = bulk sulfur content in weight fraction;
N_m = number of S atoms per metal surface atom;
A = surface area of sample (cm^2); and
W = sample weight (gm).

These are shown as dashed lines for 1 full monolayer (blue) and 10 monolayers (orange). It is interesting to see that the slopes correspond roughly to the interpolated experimental adhesion boundaries (solid). Furthermore, a segregation level accruing to about 1 monolayer can be taken as a rough criterion to define adherent behavior. This is not to say that actual interfacial segregation must reach a full monolayer at one time, but just that there is a sufficient reservoir to replenish the interface only up to one monolayer total (It is generally believed and shown that surface and interfacial segregation saturates at low monolayer levels at any one time [8,9].

The above discussion thus provides a perspective or guideline for low sulfur oxidation-resistant single-crystal superalloys. Air-cooled blades in aero-turbines typically have very thin sections, ~1–2 mm. Ground power or industrial turbines can have thicker sections, which may require more stringent sulfur limits. Nevertheless, at very low levels, $\leq$ 0.2 ppmw, thermodynamic segregation laws may limit segregation, according to the Langmuir–McLean isotherm, even for larger section thickness [8]. This behavior may be seen for the 2.5 and 5 mm ("100 mil", "200 mil") samples in the adhesion map, Figure 3.

3.5. Segregation Projections

The relation for S surface segregation in 200 ppm S Ni was obtained by Miyahara et al. [10] and generalized to all S levels as Equation (2) [8]:

$$\theta/(1-\theta) = 0.19\, C_S/(1 - C_S) \exp(137\ \text{kJ/RT}) \quad (2)$$

where θ is the surface segregation level (relative to a maximum saturation value assumed to be 0.5), and C_S is the bulk sulfur content (atomic fractions).

It was shown that between 0.1 and 10 ppma (0.06 and 6 ppmw) S, large changes in equilibrium segregation are predicted for the 900–1200 °C temperature range, covering most operational turbine airfoils. This dependency is shown in Figure 4 for 1100 °C. One can estimate the bulk sulfur content that yields a low θ = 1% surface saturation (relative to 0.5 monolayers). At 1100 °C, for example, Equation (2) yields the low bulk sulfur level of 0.33 ppma (~0.20 ppmw) S to predict low 1% segregation. Sulfur levels in this lower range should, therefore, result in minimal surface segregation, regardless of sample thickness, as indicated by the dashed horizontal line in the adhesion map of Figure 3. That is, adhesion will not be as adversely affected by larger reservoirs for thick sections at these low bulk levels. At higher amounts, ~5 ppmw, it is seen that 20% segregation is projected. Furthermore, higher temperatures retain more sulfur in solution and segregate less at the same bulk level (low temperatures project as 0.5 monolayers, i.e., full saturation, but can only occur if diffusion is sufficient). Experimentally, low surface segregation had been demonstrated below 900 °C for standard PWA 1480 at 7 ppmw S). Moreover, lower segregation had been demonstrated for PWA 1480 hydrogen desulfurized to 0.1 ppmw [8]. Interface segregation is more appropriate than surface segregation for scale adhesion issues, as demonstrated experimentally [9]. Again, lower bulk S levels were shown to produce lower S interfacial levels.

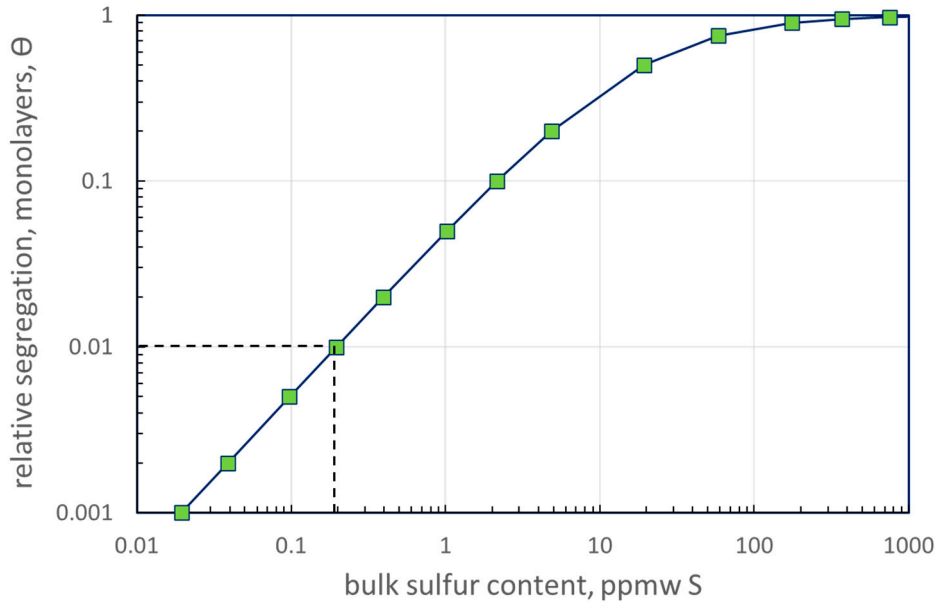

Figure 4. Projected relation between surface segregation and bulk sulfur content at 1100 °C (McLean–Langmuir isotherm, Equation (2)).

3.6. High Performing 2nd Generation Single Crystals

It is noted that some samples exhibited very adherent behavior even up to 1000 1 h cycles at 1100 °C (Table 3). While it is important here to display and map the full range of behavior over a significant range of sulfur contents, it is recognized that improved performance is observed for low sulfur Gen 2, and beyond, single-crystal superalloys. One primary reason may be the widespread use of 0.1–0.2 wt% Hf in most formulations, as well

as the absence of Ti in Rene'N5 or PWA 1484. Here, the gettering potential of Hf for S and C is expected to play an additional positive role compared to PWA 1480 having no Hf.

In that regard, we have shown very adherent behavior (+0.80 mg/cm^2) for Rene'N5 hydrogen-annealed to 0.01 ppmw S after 1000 1 h cycles at 1150 °C [11], Table 6 and Figure 5. Furthermore, PWA 1484, hydrogen-annealed to 0.01 ppmw S or melt desulfurized to 0.25 ppmw S, exhibited adherent behavior after 2000 1 h cycles at 1100 °C (+0.93 mg/cm^2 or +0.77 mg/cm^2), and after 1000 1 h cycles at 1150 °C (0.52 mg/cm^2) [12,13]. In addition, Rene'N6, hydrogen-annealed to 0.08 ppmw S, lost 0.8 mg/cm^2 after 200 h at 1200 °C [14]. These small weight changes (< 1 mg/cm^2) are among the lowest produced and recorded for these oxidation times and temperatures for single-crystal superalloys without Y-doping (They may appear exaggerated here on the highly expanded scale of Figure 5). Here sporadic maxima and abrupt drops due to moisture or water immersion (delayed spallation) are demonstrated. The best 1000 h results from PWA 1480 in this study are shown as an average of three samples, with 0.05, 0.08, and 0.28 ppmw S, samples 20-3,6,9, Table 1.

Table 6. Compilation of cyclic oxidation final weight change data for some oxidation-resistant low sulfur 2nd generation single-crystal superalloys (H, hydrogen-annealed; M, melt-desulfurized). a: Smialek 1998 [7], b: Smialek 2002 [13], c: Irvine et al. 1999 [14], d: Smialek, Pint 2001 [11], e: Smith et al. 1995 [15] f: Gray, Harris 2017 [16].

Alloy	T (°C)	t (h)	ppmw S	W/A (mg/cm^2)	Process	Study
PWA 1484	1100	2000	0.01	0.93	H	a, b
PWA 1484	1100	2000	0.25	0.77	M	a, b
PWA 1484	1150	1000	0.01	0.10	H	a, b
PWA 1484	1150	1000	0.25	0.52	M	a, b
PWA 1484	1177	600	0.2	−0.56	M	c
Rene'N5	1150	1000	0.01	0.80	H	d
Rene'N6	1200	200	0.08	−0.80	H	e
CMSX-4®(SLS)	1135	680	0.25	0.48	M	f
CMSX-4®(SLS)	1200	500	0.25	−4.90	M	f

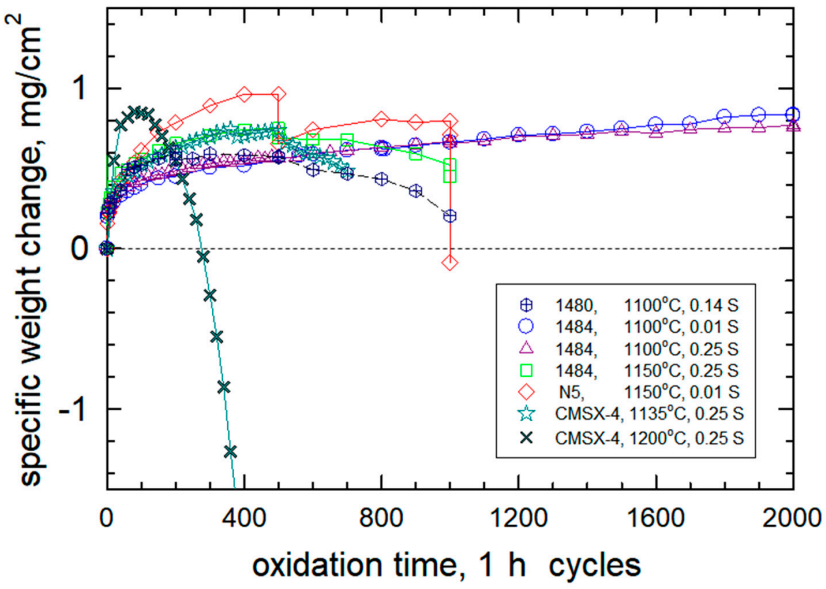

Figure 5. Representative cyclic oxidation curves for highly oxidation-resistant low sulfur 2nd generation single-crystal superalloys compared to PWA 1480 average behavior (1100 °C–1200 °C, 500–2000 h, 0.01–0.25 ppmw S).

The hydrogen-annealed samples are compared and similar to, for example, melt desulfurized 0.2 ppmw S PWA 1484 after 500 h oxidation at 1177 °C (−0.56 mg/cm^2) [15].

Additionally, melt desulfurized CMSX-4® SLS remained substantially adherent after 680 h oxidation at 1135 °C (+0.48) but somewhat compromised after 500 h oxidation in an excessive 1200 °C exposure (−4.90 mg/cm^2) [16]. The CMSX-4® SLS study applies to large commercial endeavors, where sulfur contents on the order of 0.1–0.3 ppmw, produced by CaO-based melt desulfurization, have been widely available, with over 700,000 lbs of SLS master heats delivered [17]. The commercial significance of ultra-low sulfur content Gen 2+ single-crystal superalloys has been well established by the industry.

4. Summary and Concluding Remarks

It has been recalled that undoped single-crystal superalloy compositions may exhibit excellent cyclic oxidation resistance, provided the sulfur content is very low, typically below 1 ppmw. This is compared to standard impurity contents of about 2–10 ppmw, historically. Empirically the best cyclic oxidation behavior was exhibited by a material having less than about 0.3 ppmw S, regardless of section thickness (i.e., total sulfur reservoir), with little improvement at 0.01 ppmw. An optimal 1100 °C oxidation weight change (just +0.6 mg/cm^2) was achieved for desulfurized PWA 1480 in 500 1 h cycle tests. This is compared to severe degradation (−25 mg/cm^2 losses) for standard purity material.

Surface segregation isotherms suggest that bulk sulfur levels at ~0.2 ppmw should produce less than 1% relative surface segregation. Whether 1% or 10% segregation represents a critical level is difficult to establish. Some continua of behavior were observed between intermediate levels ~0.4 to 2 ppmw. Here, transitions occurred from largely no Al_2O_3 scale spallation to gradual re-exposure of bare metal, loss of Al, and formation of less-protective $Ni(Al,Cr)_2O_4$, then Cr_2O_3 scales. Fine-tuning at these levels may be complicated by statistical variations and the accuracy limits of GDMS sulfur analyses, at one time referred to as ± 25% at low ppm S levels, with a sensitivity limit of 0.01 ppmw (10 parts per billion).

Lastly, the demonstration of excellent scale adhesion at low sulfur levels for single-crystal superalloys initially reported in 1989 [1] for 1 atm hydrogen-annealed PWA 1480 is still a matter of commercial significance. Low S, Gen 2 single-crystal superalloys have been developed and used by industry at optimal levels and remarkable cyclic oxidation performance. For example, up to 2000 1 h cycles at 1100 °C or 1000 cycles at 1150 °C have resulted in quite nominal scale growth and spallation, accruing under just 1 mg/cm^2 overall.

Funding: This research received no external funding. Source data originated under NASA Fundamental Aeronautics Program.

Institutional Review Board Statement: Not applicable.

Informed Consent Statement: Not applicable.

Data Availability Statement: Not applicable.

Acknowledgments: John Smeggil, UTRC (retired), originally encouraged us to continue low sulfur work (PWA 1480 and GDMS). Donald Lees, Manchester, is appreciated for first desulfurizing Cr by hydrogen-annealing to improve scale adhesion. At NASA, Brian Tubbs performed the first experimental study on hydrogen-annealed PWA 1480, justifying the extended program presented here, in which Donald Humphrey performed hydrogen annealing, and Douglass Jayne demonstrated surface segregation by high-temperature XPS. GDMS analyses and commentary were obtained from C. Shivakula (Shiva) and Karol Putera (EAG). Helpful guidance and 2nd Gen alloys were provided by Larry Graham, PCC and Jon Schaeffer, Wendy Murphy, GEAE. Finally, helpful discussions and CMSX-4® data were provided by Ken Harris, Cannon-Muskegon, and Simon Gray, Cranfield University.

Conflicts of Interest: The author declares no conflict of interest.

References

1. Tubbs, B.K.; Smialek, J.L. Effect of Sulfur Removal on Scale Adhesion to PWA 1480. In *Corrosion and Particle Erosion at High Temperatures*; Srinivasan, V., Vedula, K., Eds.; TMS-AIME: Warrendale, PA, USA, 1989; pp. 459–487.

2. Smialek, J.L.; Tubbs, B.K. Effect of sulfur removal on scale adhesion to PWA 1480. *Metall. Mat. Trans. A* **1995**, *26*, 427–435. [CrossRef]
3. Smialek, J.L. Oxidation Resistance and Critical Sulfur Content of Single Crystal Superalloys. *J. Engineer. Gas Turb. Power, ASME Trans.* **1998**, *120*, 370–374. [CrossRef]
4. Smialek, J.L. Effect of Hydrogen Annealing and Sulfur Content on the Oxidation Resistance of PWA 1480. *PPM. Other Propuls. R T* **1997**, *1*, 1–13.
5. Smialek, J.L. Maintaining Adhesion of Protective Al_2O_3 Scales. *JOM* **2000**, *52*, 22–26. [CrossRef]
6. Smialek, J.L. Toward Optimum Scale and TBC Adhesion on Single Crystal Superalloys. In *High Temperature Corrosion and Materials Chemistry*; Opila, E.J., Hou, P.Y., Shores, D., McNallan, M., Oltra, R., Eds.; The Electrochemical Society: Pennington, NJ, USA, 1998; Volume 98–99, pp. 211–220.
7. Smialek, J.L.; Auping, J.V. COSP for Windows: Strategies for Rapid Analyses of Cyclic Oxidation Behavior. *Oxid. Met.* **2002**, *57*, 559–581. [CrossRef]
8. Jayne, D.T.; Smialek, J.L. A Sulfur Segregation study of PWA 1480, NiCrAl, and NiAl Alloys. In *Microscopy of Oxidation II*; Newcomb, S.B., Bennett, M.J., Eds.; Institute of Metals: London, UK, 1993; pp. 183–196.
9. Hou, P.Y. Segregation Phenomena at Thermally Grown Al_2O_3/Alloy Interfaces. *Annu. Rev. Mater. Res.* **2008**, *38*, 275–298. [CrossRef]
10. Miyahara, T.; Stolt, K.; Reed, D.A.; Birnbaum, H.K. Sulfur Segregation on Nickel. *Scripta Met.* **1985**, *19*, 117–121. [CrossRef]
11. Smialek, J.L.; Pint, B.A. Optimizing Scale Adhesion for Single Crystal Superalloys. *Mater. Sci. Forum* **2001**, *369*, 459–466. [CrossRef]
12. Smialek, J.L. Scale Adhesion, Sulfur Content, and TBC Failure on Single Crystal Superalloys. In Proceedings of the 26th Annual Conference on Composites, Advanced Ceramics, Materials, and Structures: B: Ceramic En-gineering and Science Proceedings, Cocoa Beach, FL, USA, 1 January 2002; pp. 485–495.
13. Smialek, J.L. Improved Oxidation Life of Segmented Plasma Sprayed 8YSZ Thermal Barrier Coatings. *J. Therm. Spray Technol.* **2004**, *13*, 66–75. [CrossRef]
14. Smith, M.A.; Pregger, B.A. Effect of sulfur on the cyclic oxidation behavior of a single crystalline, nickel-base superalloy. *Mat. Sci. Eng. A* **1995**, *203*, 388–398. [CrossRef]
15. Irvine, J.D.; Vogt, R.G.; Bierstine, D.L.; Stabile, C.M.; Mihalisin, J.R.; Smith, J.S.; Kunkle, J.P.; Cole, G.R.; Nielsen, T.W. Ultra Low Sulfur Superalloy. US Patent 5,922,148, 13 July 1999.
16. Gray, S.; Harris, K. Cranfield and Cannon-Muskegon. Unpublished work. 2017.
17. Harris, K.; Cannon-Muskegon. Personal communication, 2020.